ACS APPLIED MATERIALS & INTERFACES

Research Article

www.acsami.org

Direct Intranuclear Anticancer Drug Delivery via Polydimethylsiloxane Nanoparticles: in Vitro and in Vivo Xenograft Studies

Gargi Mishra,[†] Souryadeep Bhattacharyya,[†] Vipul Bhatia,[§] Bushra Ateeq,[§] Ashutosh Sharma,*[,†] and Sri Sivakumar*[,†,‡]

[†]Department of Chemical Engineering, Centre for Environmental Science & Engineering, Thematic Unit of Excellence in Soft Nanofabrication, [‡]Material Science Programme, and [§]Department of Biological Sciences & Bioengineering, Indian Institute of Technology Kanpur, Kanpur 208016, Uttar Pradesh, India

Supporting Information

ABSTRACT: Direct delivery of anticancer drugs to nuclei of tumor cells is required to enhance the therapeutic activity, which can be achieved by a nuclear localization signal (NLS) or peptide-decorated nanovehicles. However, NLS/peptide-based approaches may create certain undesirable immunological responses and the utilized synthesis processes are generally labor intensive. To this end, we report ligand-free, enhanced intranuclear delivery of Doxorubicin (Dox) to different cancer cells via porous polydimethylsiloxane (PDMS) nanoparticles (NPs). PDMS NPs were prepared by sacrificial silica template-based approach and Dox was loaded into the pores of PDMS NPs. These Dox-loaded PDMS NPs show enhanced cytotoxicity and reduce the IC50 values by 84 and 54% for HeLa and PC-3, respectively, compared to free Dox. Further, DNA damage in HeLa cells was estimated using comet assay suggesting enhanced DNA damage (72%) with Dox-loaded PDMS NPs as compared to free Dox (12%). The therapeutic efficiency of PDMS-Dox drug delivery system was tested in prostate cancer (PC-3) xenografts in NOD/SCID mice which showed enhanced tumor reduction (~66%) as compared to free Dox. Taken together, our PDMS-Dox delivery system shows efficient and enhanced transportation of Dox to tumor cells which can be harnessed to develop advanced chemotherapy-based approaches to treat prostate and other cancers.

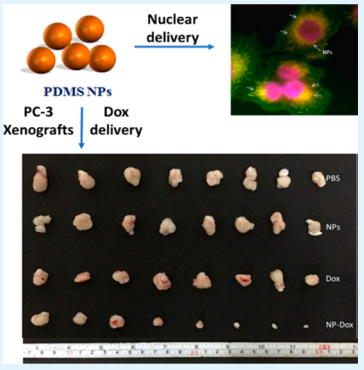

KEYWORDS: *intranuclear, doxorubicin, drug delivery, xenografts, nuclear localization signal, polydimethylsiloxane*

1. INTRODUCTION

Delivery of anticancer drugs directly to the nuclei of tumor cells can greatly enhance their therapeutic efficacy because the nucleus is the master regulator of numerous oncogenic hallmarks such as cell proliferation, apoptosis in addition to the transcriptional regulation of oncogenes or tumor suppressor genes.[1−4] Anticancer drugs can be delivered to the nuclei of cells either in a free drug form,[5] or via nanovehicles based delivery systems.[6−8] Targeting the drugs directly to the required cellular compartments like nuclei reduces their nonspecific interactions with other cytosolic components which can limit their efficiency and cause side effects.[9] This can be circumvented by delivering the drugs via nanovehicles of size less than 10 nm[10] or via nanoparticles decorated with intrinsic targeting molecules derived from biomolecules, for example, trans-activator of transcription (TAT) and nuclear localization signal (NLS) peptide sequences etc.[11−13] Though these targeted approaches show promising results, they possess following challenges: (1) Both of these approaches may lead to complexity at in vivo level by affecting the opsonisation and generation of neutralizing antibodies against intrinsically targeted molecules causing further immunological reactions;[14] (2) Surface modification of nanovehicles with targeted ligands generally involves complex and labor intensive synthesis procedures. Alternatively, a few reports are available on the delivery of anticancer drugs to nuclei via ligand-free nanovehicles. For example, Doxorubicin (Dox) was delivered to nuclei of HeLa cells through localization signal-free dextran-lipoic acid NPs and gold-dextran core−shell NPs.[15,16] In another example, graphene quantum dots have been used as a ligand-free vehicle to enhance the intranuclear accumulation of Dox in nuclei of MCF-7 and MGC-803 cells.[17] Notwithstanding this progress, it is essential to develop simple, generic and versatile ligand-free alternative nanocarriers to deliver anticancer drugs to nuclei of various cancer cells. Herein, we demonstrate the delivery of Dox via ligand-free porous PDMS NPs to nuclei of various cancer cells (e.g., HeLa, A498, HepG2, and PC-3). In addition, to test the generic nature of delivery of this reported approach, we also demonstrated delivery of the nonspecific staining dyes, e.g., fluorescein isothiocyanate (FITC) and rhodamine isothiocyanate (RITC)) to the nuclei of various cancer cells.

Received: June 19, 2017
Accepted: September 13, 2017
Published: September 13, 2017

DOI: 10.1021/acsami.7b08806
ACS Appl. Mater. Interfaces 2017, 9, 34625−34633

Polydimethylsiloxane (PDMS) polymer and its composites are widely used as matrices, membranes or coatings in drug delivery systems, blood pumps, intraocular lenses, medical adhesives, catheters, and artificial skins because of its highly biocompatible, low toxic, chemically inert, and thermally stable nature.[18−20] In general, PDMS is limited to implant-based drug delivery systems such as transurethral,[21] subcutaneous,[22] and transdermal devices.[23] It is well-known that PDMS is a very soft material and can undergo elastic deformations because of its low elastic modulus (∼1−3 MPa). PDMS, in a soft nanoparticle format, may facilitate the NPs to squeeze through the narrow pores of the nucleus and deliver the drugs. We note that soft materials like polymeric transferosomes and ultraflexible polymerosomes/liposomes have been reported to squeeze through very narrow pores of skin.[24,25] Because of its well-reported biocompatibility, FDA approval and elastic property, we were motivated to synthesize PDMS based NPs and investigated its potential as nuclear drug delivery vehicle. It is to be noted that a few reports are available on the fabrication of PDMS copolymer-based micelles and NPs for anticancer drug delivery vehicles; however, these approaches lack nuclear targeting ability.[26,27]

Herein, we report the fabrication of ligand-free PDMS NPs by sacrificial silica template-based approach for the delivery of Dox to nuclei of tumor cells. To best of our knowledge, this is the first report on the fabrication of PDMS NPs for nuclear drug delivery applications. Dox-loaded PDMS NPs showed enhanced cytotoxicity and reduced the IC50 values of IC50 values by 84%, and 54% for HeLa and PC-3 cells respectively when compared to free Dox. Dox-induced DNA damage was assessed by comet assay which showed 72% and 12% DNA damage with PDMS-Dox and free Dox respectively elucidating the enhanced anticancer activity of PDMS-Dox nanoparticle. Further, delivery of Dox to the nucleus was confirmed by confocal and electron microscopy images.

Further, we tested PDMS-Dox delivery system in aggressive PC-3 prostate cancer xenografts in mice tumor models. The experimental mice administered with PDMS-Dox system showed a significant reduction (∼3 folds) in the tumor burden as compared to free Dox group, suggesting the enhanced therapeutic efficacy of our delivery system. In order to prove the generic nature of delivery ability of PDMS NPs to nuclei was further validated by the delivery of nonspecific staining dyes (FITC and RITC).

2. RESULTS AND DISCUSSION

2.1. Synthesis of PDMS Nanoparticles. The porous PDMS NPs were prepared by a template-based approach using solid core-mesoporous shell (SCMS) silica as a sacrificial template (as shown in Scheme 1).[28,29] SCMS particles were synthesized by adapting the procedure reported by Unger et al.[30] SCMS silica particles possess a Brunauer−Emmett−Teller (BET) surface area of 369.5 m^2/g with average pore diameter of 3.4 nm. SCMS particles were infiltrated with PDMS polymer followed by curing at 100 °C. The silica part in the PDMS-SCMS particles (∼330 nm) was etched by hydrofluoric acid (HF) treatment leading to the formation of PDMS NPs (denoted as bare PDMS NPs). Figure 1 a shows scanning electron microscopy (SEM) image of bare PDMS particles suggesting their monodispersity with the size of ∼200 nm which was further validated by the transmission electron microscopy (TEM) images (Figure 1 b). We note that there is a reduction in the size of bare PDMS NPs compared to SCMS

Scheme 1. Fabrication of PDMS NPs for Nuclear Delivery of Anticancer Drugs and Dyes

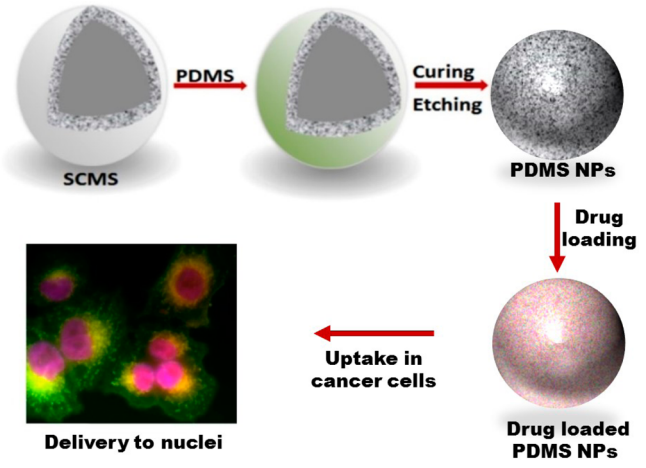

NPs. In addition, it is interesting to note that the bare PDMS NPs did not form as hollow capsule unlike other polymer capsules formed from the similar size of SCMS template. We believe that the cured polymer after etching does not retain its shape as a capsule and hence collapses to form a particle. We note that cross-linking in the confined pores of silica facilitates the formation of PDMS polymer as nanoparticles. Also, we can see that PDMS NPs are not uniformly spherical in their shape which can be attributed to the flexible elastomeric properties of PDMS polymer.

Further, TEM images suggest that bare PDMS particles possess porosity whereas Dox-loaded PDMS particles show lesser porosity due to infiltration of Dox into pores (Figure 1 c). It is to be noted that we are unable to estimate the BET surface due to the requirement of a large amount of sample for measurements. Further, the energy dispersive analysis of X-rays (EDAX) data (Figure S1a) shows the presence of carbon along with silicon and oxygen confirming the formation of PDMS NPs. The Fourier transform infrared spectra (FTIR) spectra (Figure S2) of the SCMS silica template shows major peaks at 807 and 1086 cm^{-1} which can be attributed to Si−O symmetric and asymmetric vibrations, respectively. In comparison to the bare SCMS silica template, bare PDMS NPs show additional peaks at 970 cm^{-1} (=C−H bending vibrations), 1626 cm^{-1} (C=C stretching of vinyl group's of Sylguard 184) which further confirms the formation of PDMS particles.[31] Zeta potential measurement suggests that bare PDMS NPs are negatively charged (−12.13 mV). Further, dynamic light scattering (DLS) measurement (Figure S3) demonstrates that bare PDMS particles possess the average hydrodynamic diameter of ∼290 nm which is higher as compared to electron microscopic results, which may be attributed to the swelling of PDMS particles in aqueous media. For drug delivery applications, accurate control of size and porosity of nanoparticles is very important. Because we have used a template-based synthesis of PDMS NPs, we can change the size of SCMS template to control the size and control the porosity by changing the concentration of the porogen.

2.2. Loading of Dox on PDMS Nanoparticles and Release Kinetics. In order to understand the drug release profile, we have performed in vitro drug release studies of Dox-loaded PDMS NPs in PBS (pH 7.4) at 25 °C. Figure S4 shows cumulative nonlinear release profile of drug from PDMS NPs

DOI: 10.1021/acsami.7b08806
ACS Appl. Mater. Interfaces 2017, 9, 34625−34633

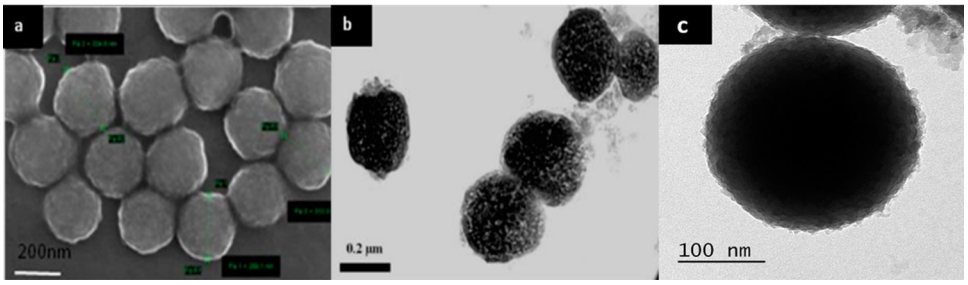

Figure 1. (a) SEM, (b) TEM image bare PDMS NPs, and (c) TEM image of Dox-loaded PDMS NPs.

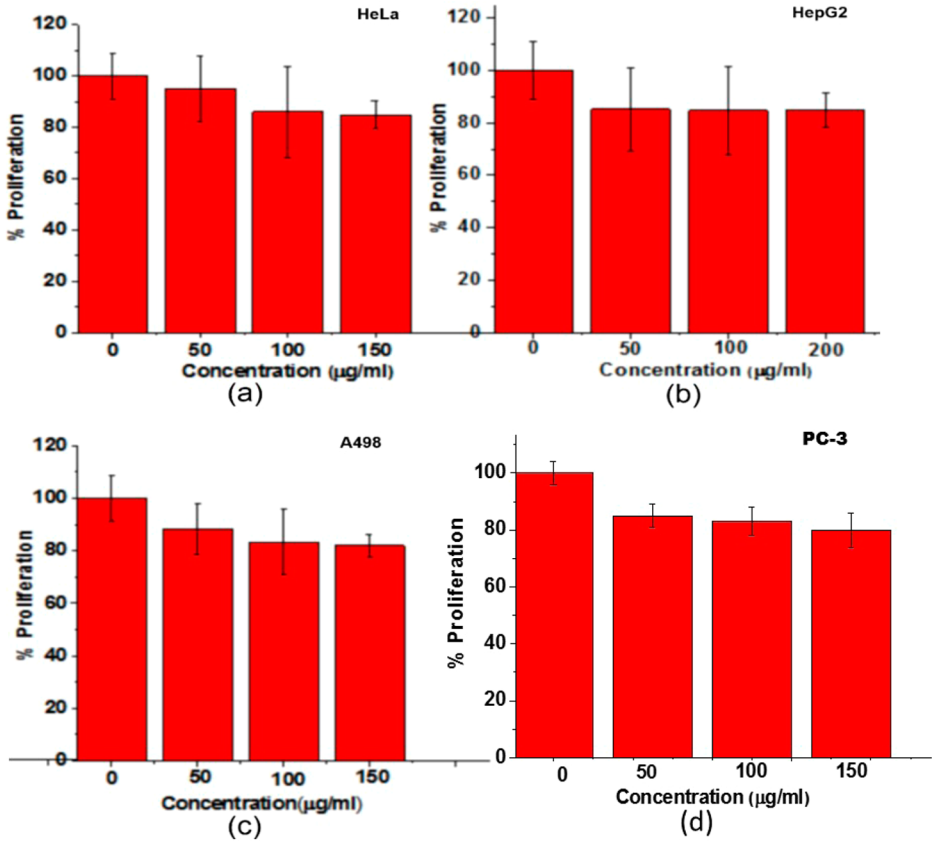

Figure 2. Biocompatibility of bare PDMS NPs on cancer cell lines; (a) HeLa, (b) HepG2, (c) A498, and (d) PC-3.

for a time period of 25 h. It is observed from release profile that ~50% of the drug was released in first 10 h and the remaining amount was released slowly thereafter. The calibration curve of optical density vs concentration Dox dissolved in PBS buffer was plotted to quantify the drug release (Figure S5). This drug release profile can be attributed to the drug released by diffusion of the drug from external surface pores of the PDMS NPs followed by the drug release from the polymeric matrix of PDMS NPs.

2.3. PDMS Nanoparticles Do Not Cause Cytotoxicity and Enhance the Therapeutic Efficacy of Dox against Tumor Cell Lines. Prior to any therapeutic application, it is important to analyze the cytotoxicity of the bare PDMS NPs on the viable cells. Therefore, 3-(4,5-dimethylthiazol-2-yl)-2,5-diphenyltetrazolium bromide (MTT) assay was conducted to investigate in vitro biocompatibility of bare PDMS NPs. MTT assay was performed using different concentrations of bare PDMS NPs with HeLa, A498, HepG2, and PC-3 cancer cells. MTT assay clearly suggests that bare PDMS NPs are highly biocompatible within a concentration range of 0−150 μg/mL suggesting that PDMS NPs can be used as a delivery carrier (Figure 2).

To evaluate the therapeutic efficiency of Dox-loaded PDMS NPs, we performed MTT cytotoxic assays along with free Dox as a positive control. The amount of drug loaded on the PDMS NPs for different doses (0−100 μg/mL) were calculated (Tables S1 and S2) and accordingly, the equal amount of free Dox was added to the HeLa, A498, HepG2 and PC-3 cells. Decrease in IC50 values for Dox delivered via PDMS NPs toward various cell lines are A498 (0.18 μM), HeLa (0.18 μM), HepG2 (0.2 μM) and PC-3 (1.14 μM) was observed as compared to cells treated with free Dox HeLa (1.12 μM), A498 (0.24 μM), HepG2 (0.72 μM) and PC-3 (2.47 μM) (Figure 3, Figures S6−S9). This clearly suggests that Dox delivered via PDMS NPs show greater cytotoxicity as compared to the free drug and reduces the IC50 values by 84, 54, and ~72% for HeLa, PC-3, and HepG2 cells, respectively.

DOI: 10.1021/acsami.7b08806
ACS Appl. Mater. Interfaces 2017, 9, 34625−34633

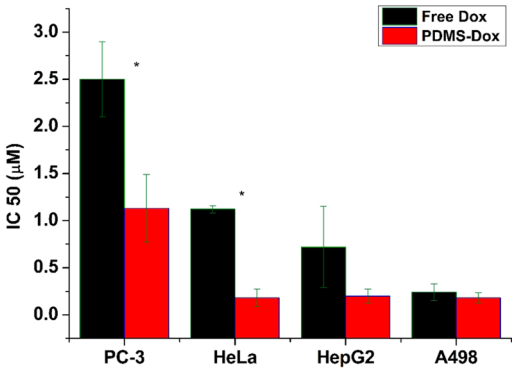

Figure 3. Comparison of the IC50 value of free Dox and Dox-loaded on PDMS NPs. IC50 line graph of PDMS-Dox on PC-3, HeLa, HepG2, and A498 are given in Figures S6–S9 (p values are 0.0116 and 0.0154, respectively).

However, the very minimal difference was observed in A498 cells which need further exploration. It can be concluded that the PDMS NPs hold good promise for being used as a drug delivery vehicle for anticancer drugs against cancer cells.

2.4. PDMS Nanoparticles Enhance the Perinuclear and Nuclear Accumulation of Dox/Dyes in Cancer Cells. To have good therapeutic efficiency, a drug delivery agent should be capable of crossing the cell membrane and reach the desired intracellular destination. To assess the uptake of PDMS-Dox, PDMS-FITC, and PDMS-RITC NPs, cell uptake studies were conducted on HeLa cells, HepG2, and A498 cells and were analyzed using fluorescence and confocal laser scanning microscopy as shown in Figure 4. Nuclear localization of PDMS NPs can be clearly seen as the accumulation of red/green fluorescence of Dox/RITC/FITC-loaded NPs inside the nuclei and near nuclear membrane and pores (Figure 4 and Figure S10). In contrast, the fluorescence signals were distributed in all over cells in the case of free Dox, FITC and RITC (Figure S11) suggesting the targeting ability of PDMS NPs. This suggests that the successful delivery of Dox through PDMS NPs to the nuclei of cancer cells without utilizing any extrinsic ligand and targeting agents.

A detailed view of PDMS-RITC associated with the nuclear membrane and accumulated inside the nuclei of HeLa cells can be seen in Figure 4. Similarly, cellular internalization of PDMS-FITC NPs was also observed in HepG2 and A498 cells (Figure S12). In HepG2, the majority of particles are accumulated around the nuclei. In A498 cells, the nuclear localization is lesser as compared to Hela and HepG2 cells which might be a cause of reduced efficacy of this delivery vehicle in this particular cell line though it needs further exploration. We investigated the intranuclear localization of PDMS-Dox NPs in prostate cancer cells (PC-3) and it showed nuclear uptake in the cells as shown in Figure 5; however, it was less prominent as compared to HeLa cells. It is to be noted that prostate cancer cell lines like PC-3 show resistance toward anticancer drugs because of excess expression of P-glycoprotein and multiple drug resistance protein which might be the reason for reduced PDMS-NPs uptake.[32] We later on used the PC-3 cells to generate xenograft models for in vivo testing of PDMS-Dox as intranuclear drug delivery agent.

To understand the fate of PDMS NPs inside the cells, we observed internalization of PDMS NPs in HeLa cells using

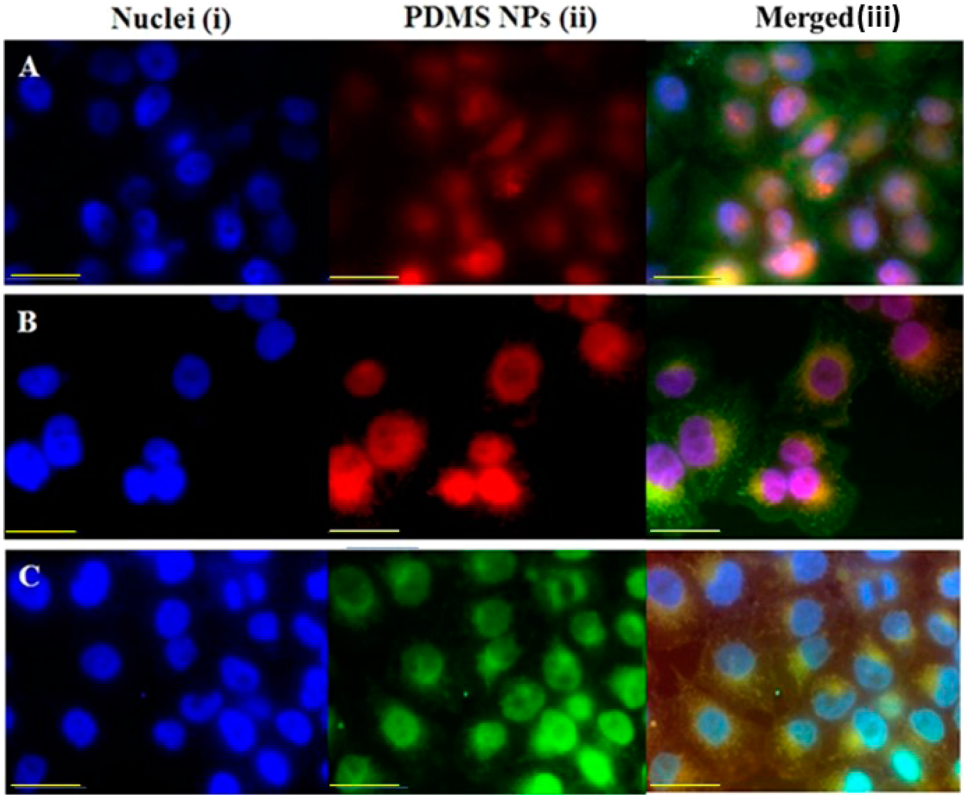

Figure 4. Cellular internalization of PDMS NPs in HeLa cells; (A) (i) nuclei-Hoescht, (ii) PDMS-Dox, and (iii) merged image; panel B) (i) nuclei-Hoescht, (ii) PDMS-RITC and (iii) merged image; panel C) (i) nuclei-Hoescht, (ii) PDMS-FITC, and (iii) merged image; scale bar represents 20 μm.

DOI: 10.1021/acsami.7b08806
ACS Appl. Mater. Interfaces 2017, 9, 34625–34633

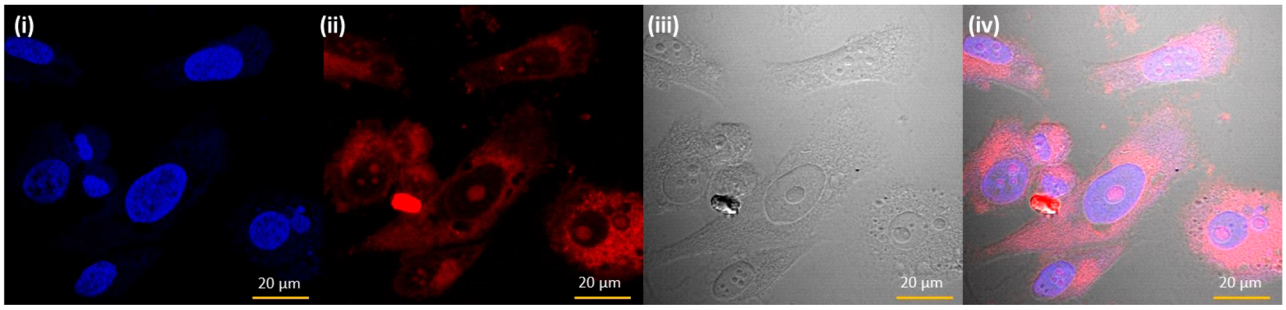

Figure 5. PDMS-Dox internalization in PC-3 cells; (i) nuclei-Hoescht, (ii) PDMS-Dox and (iii) PC-3 cells DIC image, and (iv) merged images.

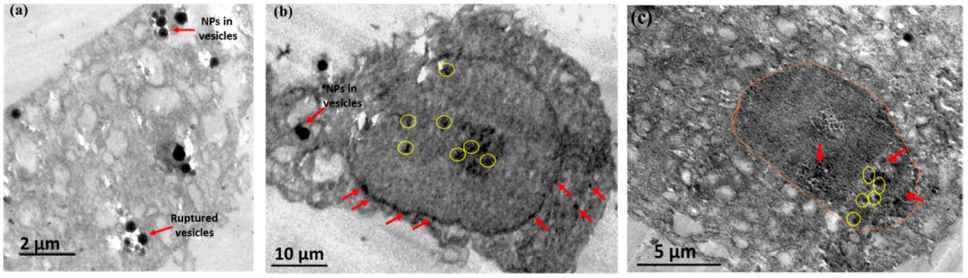

Figure 6. TEM images showing different stage of PDMS NP internalization inside the HeLa cells. (a) Localization of PDMS NPs in endosomal vesicles (after 2 h), (b) nuclear localization of PDMS NPs (after 12 h), and (c) detailed view of cells showing nuclear localization.

TEM after 2 and 12 h as shown in Figure 6a and b. After 2 h, internalized PDMS NPs can be seen near the plasma membrane entering via endosome-like vesicles as shown in Figure 6 a. It is observed that PDMS NPs (black dots denoted by red arrows) have been engulfed inside endosomes after 2 h. Figure 6b, c clearly suggests that the PDMS nanoparticles were located in perinuclear (red arrwows) and intranuclear region (yellow circle). In addition, PDMS NPs can be seen near the ruptured endosomes suggesting the early endosome escape. It is worthy to note that the size of PDMS particles (<100 nm) present in the perinuclear and intranuclear region is smaller while compared to particles present in the early endosomes. We propose that PDMS NPs can escape out of endosome because of proton sponge effect owing to the swelling of the PDMS polymer in acidic pH condition of endosomes.[33] This effect may lead to release of NPs in the cytoplasm which can get transported to perinuclear region and facilitate the entry of PDMS NPs inside the nuclei as observed from Figure 6 b and c. From these results we hypothesize that the nuclear localization may be due to the low elastic modulus of PDMS and degradation of PDMS (after early endosome escape). Please note that the reasons provided above are based on our preliminary observations. In order to confirm the mechanism/reason we have planned the following future experiments: (1) varying the size of PDMS nanoparticles, (2) varying the elastic modulus pf PDMS by controlling the degree of cross-linking, (3) understanding the nuclear uptake mechanism using different inhibitors, etc.

2.5. PDMS-Dox Show Increased DNA Damage As Compared to Free Dox. Most of the effective anticancer drugs have DNA-damaging properties. It is well-known that Dox intercalates in DNA bases and poisons topoisomerase-II leading to DNA damage and cell death. Thus, to investigate the DNA damage caused by Dox–loaded PDMS NPs, comet assay was performed. DNA quantification in the comet tails represents single and double stranded breaks caused by the drug. Thus, enhanced delivery of Dox and its intercalation in the DNA base pairs is directly proportional to DNA present in the comet tail. Our comet assay data suggests that ~75% tail DNA is observed in the case of Dox-loaded PDMS NPs (25 μg/mL,) treated cells, whereas 12% of tail DNA is observed in the cells treated with the same amount of free Dox suggesting the efficacy of the delivery vehicle (Figure 7). This shows that

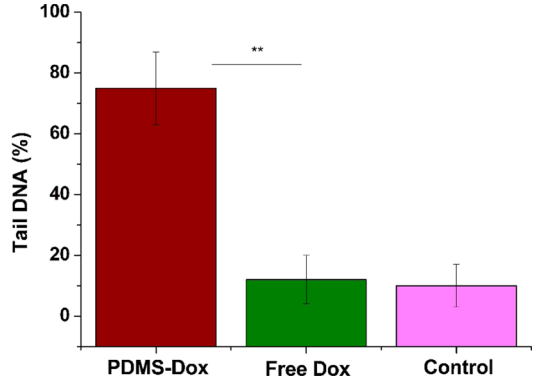

Figure 7. Tail DNA (%) of PDMS-Dox and free Dox-treated HeLa cells. The amount of Dox present on PDMS NPs was (0.14 μg) and a similar amount of free Dox was used to compare the DNA damage in both cases. Control was HeLa cells grown in the similar culture media without Dox and NPs (p-value is 0.0016).

PDMS NPs can increase the efficacy of the DNA damage by Dox by ~6 fold, which is corroborated by the cytotoxicity data discussed in section 2.3. Taken together, our data clearly suggest that PDMS delivers Dox to the nucleus with better efficiency as compared to free Dox.

2.6. Dox-Loaded PDMS Nanoparticles Show Increased Therapeutic Efficacy and Regress Tumor Burden in PC-3 xenografts. To test the therapeutic efficacy of PDMS nanoparticles as drug delivery carriers, we developed PC-3 cells xenograft in NOD/SCID mice. PC-3 are aggressive metastatic prostate cancer cells and androgen signaling

DOI: 10.1021/acsami.7b08806
ACS Appl. Mater. Interfaces 2017, 9, 34625−34633

independent. Our approach provides credible predictive response values in correlation to the clinically relevant doses. We injected the prostate cancer cells subcutaneously in NOD/SCID mice and allowed the tumor volume to reach 100 mm^3. Dox-loaded PDMS nanoparticles were initially administered at a dose of 8 mg/kg for 35 days.

PDMS-Dox group did not show any noticeable increase in the tumor volume as compared to the initial tumor volumes whereas free Dox showed an increase in the tumor volume as shown in Figure 8a, b. There was a 25 and 75% decrease in the

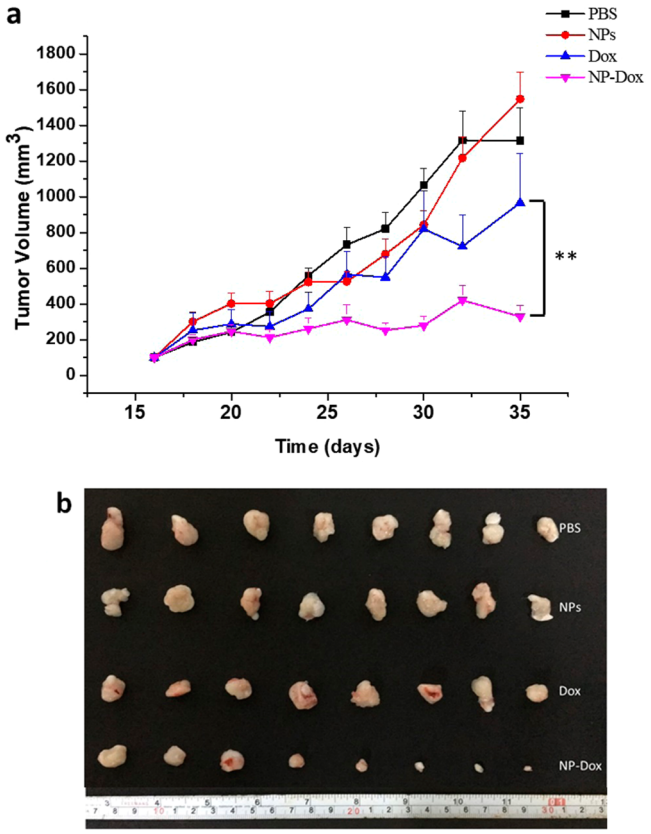

Figure 8. (a) Tumor volume (mm^3) vs time plot after giving intratumoral injections to mice; (b) representative image showing the sizes of tumors of four groups after sacrificing the mice on the 35th day (p-value is 0.0041).

tumor burden in the free Dox and PDMS-Dox group respectively, in comparison to PBS control group. It is to be noticed that in PDMS-Dox group a significant reduction was observed, ~3-fold more, as compared to free Dox group ($p < 0.05$, 0.0041). We attribute the enhanced antitumor activity to the PDMS NPs accumulating in the perinuclear and nuclear regions, which can be the cause of the increased delivery of Dox to the nuclei as validated by the in vitro experiments as well.

3. CONCLUSION

In conclusion, we have fabricated highly biocompatible porous PDMS NPs (~200 nm) as a versatile vehicle to deliver anticancer drugs to the nuclei of tumor cells without utilizing any intrinsic ligands. From the confocal images, it is clearly evident that the Dox has been delivered to nucleus efficiently compared to free Dox. Dox-loaded PDMS NPs show enhanced cytotoxicity and reduce the IC50 values of Dox by 84% and 54% for HeLa and PC-3 respectively. Furthermore, enhanced DNA damage (tail-DNA %) is observed (72%) in the case of PDMS-Dox as compared to 12% caused by free Dox suggesting better delivery by PDMS NPs. The localization of Dox fluorescence at nuclei and DNA damage of cancer cells warrant its application as advanced nuclear drug delivery systems. The therapeutic efficiency of PDMS-Dox drug delivery system was tested in prostate cancer (PC-3) xenografts in NOD/SCID mice which showed enhanced tumor reduction (~66%) as compared to free Dox. This vehicle can also be potentially used for transfection of the gene, growth factor and delivery of drugs to the nuclei of the mammalian tumor cells. As the mechanism of uptake still remains unexplored, we further need to explore the translocation pathway to harness the system in a better way.

4. EXPERIMENTAL SECTION

4.1. Materials. Tetraethyl orthosilicate (TEOS), n-octadecyltrimethoxysilane (C-18 TMS), fluorescein isothiocyanate (FITC), rhodamine-isothiocyanate (RITC), FITC-phalloidin, trypsin- ethylenediaminetetraacetic acid (trypsin-EDTA), Dulbecco's modified eagle's medium (DMEM), penicillin-streptomycin antibiotic, 3-(4,5-dimethylthiazol-2-yl)-2,5-diphenyltetrazolium bromide (MTT), gelatin (from cold water fish skin), Triton-X and Doxorubicin hydrochloride (Dox) were purchased from Sigma-Aldrich. Low melting point agarose (LMPA) was obtained from Himedia. Tetrahydrofuran (THF), ethanol, tris-base, ethylenediaminetetraacetic acid (EDTA) and dimethyl sulfoxide (DMSO) were obtained from Merck Chemicals, India. Hydrofluoric acid (HF) and ammonium fluoride (NH_4F) were obtained from SD. Fine Chemicals Limited. Sodium chloride, sodium hydroxide (NaOH pellets), methanol and acetone were purchased from Fisher Scientific. All the above chemicals were used as received. HeLa, A498, and HepG2 cells were purchased from National Centre for Cell Science, Pune, India. Araldyte CY212 epoxy resin was provided by β-Tech Limited, India.

4.2. Characterization of NPs. PDMS NPs were characterized using Scanning Electron Microscopy (SEM) (SUPRA 40 VP Gemini, Zeiss, Germany) at an accelerating voltage of 10 kV and Transmission Electron Microscopy (TEM) (FEI Technai G2 U-Twin) at 200 kV. For the microscope analysis, PDMS NPs (500 μg) were dispersed in 1 mL of water and sonicated for 5 min and 10 μL of this suspension was dried onto a silicon substrate and carbon-coated TEM grid (mesh size 200) for SEM and TEM analysis, respectively. The hydrodynamic diameter of the PDMS nanoparticles was determined by Zetasizer Nano series, NanoZS90, Malvern. Thermoscientific Multiskan Spectrum (UV−vis spectrometer) and Edinburg fluorescence spectrometer (FLSP920) were used for absorption measurements. Olympus Ix81 motorized inverted microscope and Zeiss LSM 710 confocal microscope were used for NPs and cells imaging.

4.3. Synthesis of SCMS Silica Particles. Absolute ethanol (74 mL) was added to deionized water (10 mL) in a round-bottom flask. Aqueous ammonia (25%) (12.7 mL) was slowly added to the above mixture under constant stirring at 30 °C. Tetraethylorthosilicate (TEOS, 5.9 mL) was rapidly added to the above mixture under vigorous stirring and kept for 1 h under mild stirring condition. A mixture of TEOS (0.022 mol, ~ 5.013 mL) and n-octadecyltrimethoxysilane (C-18 TMS) (1.038 mL) was added slowly to the above mixture and allowed to stir for 20 min. It should be noted that the round-bottom flask was closed during the reaction to prevent the loss of volatile ammonia. After 20 min, the mixture was incubated for one h without stirring, followed by removal of the solvent in a rotary evaporator at 60 °C. The white silica powder was obtained and was dried overnight in an oven at 100 °C followed by calcination at 550 °C for 6 h to remove the porogen.

4.4. Preparation of PDMS Stock Solution. Base component (Part A) of the commercial PDMS elastomer kit Sylguard 184 was vigorously mixed with its curing agent (Part B) in the ratio of 10:1 as advised by the manufacturers. Tetrahydrofuran (THF) (100 mL) was added to the above mixture and allowed to stir for 90 min to form 50 mg/mL PDMS stock solution.

DOI: 10.1021/acsami.7b08806
ACS Appl. Mater. Interfaces 2017, 9, 34625−34633

4.5. Synthesis of PDMS NPs. The SCMS silica template (10 mg) was sonicated with PDMS stock solution (2 mL) in a centrifuge tube for 10 min and allowed to incubate for 16 h in rotor spin. The suspension was centrifuged at 6500 rpm and followed by a washing with THF (one time) to remove unadsorbed PDMS. The prepared PDMS infiltrated silica particles were cured at 100 °C for 9 h. Finally, silica templates were removed by etching with ammonium fluoride buffered HF (1:4) solution followed by repeated washings with deionized water to remove the components of etching buffer.

4.6. Cytotoxicity Assay and IC50 Value Calculation on Cancer Cell Lines. Cytotoxicity was measured using a modified MTT assay previously described by Mosmann.[34] HepG2 cells (Human liver cancer), A498 cells (human kidney sarcoma cells) and HeLa cells (human cervical cancer cells) and PC-3 cells (prostate cancer cells) (10^4 cells per well) were seeded in 96 well tissue culture plates having a media volume of 300 μL. The seeded cells were incubated for 5 h to allow cell adhesion to the plate surface. After cell's attachment to the surface, different concentration (0- 150 μg/mL) of sonicated and sterilized PDMS NPs were added to the 96 well plates. After an incubation of 18 h, media of the wells was discarded from each well. The MTT reagent 200 μL (0.5 mg/mL) was dissolved in plain DMEM and added to each well and incubated for 4 h. MTT reagent was removed from the wells followed by the addition of 200 μL of dimethyl sulfoxide (DMSO). The plates were then incubated for 15−20 min and the optical density of the resultant complex was read spectrophotometrically at 570 nm using pure DMSO as a blank. The control for the experiment was established by seeding the similar number of cells on 2D in tissue culture treated well plates without adding NPs.

For IC50 value assessment, 1×10^4 cells per well were seeded in 96-well tissue culture plates having a media volume of 300 μL. The seeded cells were incubated for 5 h to allow cell adhesion to the plate surface. After cell's attachment to the surface, different concentration (0−100 μg/mL) of PDMS-Dox NPs were added to the 96 well plates. PDMS-Dox NPs and free Dox were added to different wells of plates and incubated for 48 h in the incubator. For HeLa, HepG2 and A498 cells, PDMS-Dox NPs with 6% Dox loading (w/w) and for PC-3 cells PDMS NPs with 8.5% Dox loading (w/w) were taken (details of samples are given in Table S1 and S2). The amounts of Dox on PDMS-Dox NPs were calculated and similar amounts of free Dox was added as a control for the comparison of cytotoxicity. After 48 h, media was removed and MTT reagent 200 μL (0.5 mg/mL) was added to each well and incubated for 4 h. MTT reagent was removed from the wells followed by the addition of 200 μL of dimethyl sulfoxide (DMSO). The plates were then incubated for 15−20 min and the optical density of the resultant complex was read spectrophotometrically at 570 nm using pure DMSO as a blank.

4.7. Drug Loading and Release Kinetics Study. Aqueous PDMS nanoparticle suspension (100 μL, 100 μg/mL) was mixed with aqueous solution of Doxorubicin (100 μL, 1 mg/mL) for 24 h at 25 °C. The mixture was centrifuged and washed with water to remove the free drug. The Dox loading was estimated by UV−vis spectroscopy measuring Dox absorbance at 550 nm. The Dox-loaded PDMS NPs were dispersed in 1 mL of PBS buffer (pH 7.4) and were incubated at 37 °C under stirring conditions (20 rpm) to study in vitro drug release kinetics. At specific time intervals, 50 μL of the buffer medium was withdrawn after centrifugation and 50 μL of fresh buffer was replenished to keep the total volume constant. The amount of Dox in the medium was determined using UV−vis absorption spectroscopy.

4.8. Internalization of Dox-Loaded PDMS NPs by Cancer Cells. Cells (HeLa, A498, HepG2 and PC-3) were cultured in tissue culture flasks and trypsinized. 1×10^4 cells (counted using a hemocytometer cell counter) were seeded on gelatin-coated coverslips kept in each well in a 24 well tissue culture plate. Cells were allowed to adhere on the coverslips for 4 h under favorable conditions. Sterilized Dox-loaded PDMS NPs (100 μg/mL) in 500 μL of complete DMEM was then added to each well. The system was left in a CO_2 incubator for 18 h in an atmosphere of 5% CO_2. After 18 h, coverslips were taken out and washed multiple times with PBS to remove free NPs present outside the cells. Fixation of cells on the coverslip substrate was done with 4% formaldehyde solution for 30 min. The cytoskeleton of the fixed cells was stained with diluted FITC-phalloidin (10 μg/mL) in PBS for 20 min at room temperature. Under an excitation wavelength ~490 nm, its emission band was observed around 525 nm. After cytoskeletal staining, cells were incubated in 200 μL of diluted Hoescht stain in PBS for 10 min to stain the nuclei. The nuclear staining was observed at different magnifications at an excitation wavelength ~346 nm and its emission band was observed around 420 nm. Doxorubicin loaded NPs were visible at an excitation ~484 nm and emission band around 580 nm. The images were merged to get a composite picture using ImageJ software. The fixed cells were monitored using an Olympus 1 × 81 fluorescence microscope and a Confocal microscope (Leica TCS SP5). A similar protocol was followed for analyzing the internalization of PDMS-FITC and PDMS-RITC NPs.

For electron microscopy, HeLa cells (10^6) were seeded in DMEM media in a Petri plate (90 mm) and after 12 h, PDMS NPs (100 μg/mL) were added to it. After 24 h of incubation, these cells were fixed with 2.5% glutaraldehyde for 2 h and washed with PBS thrice. Cells were scrapped out from the flask after fixation and pelleted down in a centrifuge tube at 1500 rpm for 3 min. This pellet was counterstained with osmium tetraoxide (0.5%) for 30 min at room temperature. The obtained pellet was dehydrated using different concentrations of acetone (30%, 50%, 70%, 90% and 100%), each for 30 min. This step was followed by dehydration using dry acetone for 30 min and clearing using toluene (100%) for 1 h. The obtained pellet was embedded in Araldyte CY212 (epoxy-based) resin and the embedding protocol was used as provided by the manufacturers. The obtained embedded samples were sliced using ultramicrotome and section of thickness 60−100 nm were obtained. These sections were placed on copper grids (200 mesh size) and observed after under high-resolution tunneling electron microscope (HR-TEM), FEI Titan G2 60−300 microscope, at an accelerating voltage of 200 kV.

4.9. DNA Damage Assay. 1×10^6 HeLa cells were cultured in 12 well tissue culture plate in complete DMEM. At 80% confluence, cells were administered 25 μg/mL PDMS-DOX NPs. The amount of Dox-loaded on 25 μg/mL PDMS-DOX NPs was calculated and the same amount (0.14 μg) of free Dox were administered to cells. A negative control was also taken which contained the same number of cell only, without any drugs and nanoparticles. After 18 h incubation, the culture media was pipetted out and cells in each well were harvested to get single-cell suspensions by trypsinization. Suspensions from each well were mixed with molten low melting point agarose (LMPA) in a ratio of 1:10 (v/v) (10 μL cell suspension, 100 μL of LMPA. Slides were labeled and 50 μL of the mixture was immediately pipetted onto clean glass slides. The slides were then placed in a dark refrigerator at 4 °C for 15 min. The slides were then immersed in a prechilled lysis solution and placed back in the refrigerator for at least 1 h. The lysis buffer was then removed and the slides were immersed in the alkaline unwinding solution for 20 min in the dark at room temperature. The slides then were removed from the alkaline unwinding solution and electrophoresed at 0.7 V/cm for 30 min in a dark room. After the electrophoresis, the slides were soaked three times in neutralizing buffer (0.4 M Tris, adjusted to pH 7.5 with HCl) for 5 min each and then immersed in 100% ethanol for 5 min. The slides were then allowed to dry before being stained with 100 mL of diluted ethidium bromide (10 μg/mL) for 5 min in a dark refrigerator. The slides were then analyzed using a fluorescent microscope at 40× and Comet IV digital imaging software. The comet tail lengths were digitally analyzed and scored based on tail length, width, and intensity. Percent of DNA (%) present in the tail is calculated by dividing the amount of DNA in the tail by the total amount of DNA associated with a cell multiplied by 100. Tail DNA (%) was used to analyze the DNA damage using the software Comet 5.0. Lysis solution, neutralization buffer, and electrophoresis buffer were prepared as reported in the literature.[35]

4.10. In Vivo Mouse Tumor Xenograft Model. All animal experiments reported in this article were done following the protocol approved by IEAC (IITK/IAEC/2016/1051) and CPSEA (IITK/IAEC/2016/1051). PC-3 cells (1 million) were injected subcuta-

DOI: 10.1021/acsami.7b08806
ACS Appl. Mater. Interfaces 2017, 9, 34625−34633

neously in 6−8 week-old male NOD/SCID mice. Tumors sizes were measured using digital Vernier caliper and volumes were calculated. Mice were randomized and distributed in four groups (5 mice/group), once the average tumor volume reached a size of 100 mm^3. Mice were treated with PBS, only nanoparticles (Dose), only DOX (Dose), PDMS-Dox (Dose) intratumorally up to 35 days. The first group was given intratumoral injections of PDMS-Dox at a dose of 4 mg/kg body weight (50 μL, injection volume) three times a week for 35 days. Likewise, respective control groups of free Dox, PDMS nanoparticles, and PBS were also injected intratumorally.[36,37] Drug treatment was initiated once average volume in each group reached ∼100 mm^3. Error bars represent mean ± s.e.m. *P*-values were derived from two-sided Student's *t* test and one-way ANOVA using GraphPad Prism software.

■ ASSOCIATED CONTENT

Supporting Information

The Supporting Information is available free of charge on the ACS Publications website at DOI: 10.1021/acsami.7b08806.

Details of samples used for cytotoxicity experiments; EDAX, FTIR, and DLS of PDMS NPs; drug release kinetics of PDMS-Dox NPs, calibration curve of Dox; IC50 curves of PDMS-Dox against A498, HepG2, HeLa, and PC-3 cell lines and confocal microscopic images of PDMS NP internalization inside different cells lines (PDF)

■ AUTHOR INFORMATION

Corresponding Authors

*E-mail: ashutos@iitk.ac.in.

*E-mail: srisiva@iitk.ac.in.

ORCID

Sri Sivakumar: 0000-0002-6472-2702

Notes

The authors declare no competing financial interest.

■ ACKNOWLEDGMENTS

This work was conducted in Indian Institute of Technology, Kanpur (India). S.S and A.S. acknowledge DST Nano mission for funding. B.A. is an Intermediate Fellow of the Wellcome Trust/DBT India and is thankful to Wellcome Trust/DBT India Alliance grant (IA/I(S)/12/2/500635) to B.A. We acknowledge Dr. Rajan Singh for his generous help in in vivo experiments. We acknowledge Rahul Bhardwaj, Advanced Imaging Centre, Indian Institute of Technology, Kanpur (India), for his help in TEM sample preparation and imaging. We acknowledge Department of Biotechnology, India, for funding the project.

■ REFERENCES

(1) Xu, P.; Van Kirk, E. A.; Zhan, Y.; Murdoch, W. J.; Radosz, M.; Shen, Y. Targeted Charge-Reversal Nanoparticles for Nuclear Drug Delivery. *Angew. Chem., Int. Ed.* **2007**, *46*, 4999.

(2) Liu, J.-n.; Bu, W.; Pan, L.-m.; Zhang, S.; Chen, F.; Zhou, L.; Peng, W.; Shi, J. Simultaneous Nuclear Imaging and Intranuclear Drug Delivery by Nuclear-Targeted Multifunctional Upconversion Nanoprobes. *Biomaterials* **2012**, *33*, 7282.

(3) Artavanis-Tsakonas, S.; Rand, M. D.; Lake, R. J. Notch Signaling: Cell Fate Control and Signal Integration in Development. *Science* **1999**, *284*, 770−776.

(4) Zink, D.; Fischer, A. H.; Nickerson, J. A. Nuclear Structure in Cancer Cells. *Nat. Rev. Cancer* **2004**, *4*, 677−687.

(5) Dalmark, M.; Storm, H. A Fickian Diffusion Transport Process with Features of Transport Catalysis. Doxorubicin Transport in Human Red Blood Cells. *J. Gen. Physiol.* **1981**, *78*, 349.

(6) Dam, D. H. M.; Lee, J. H.; Sisco, P. N.; Co, D. T.; Zhang, M.; Wasielewski, M. R.; Odom, T. W. Direct Observation of Nanoparticle−Cancer Cell Nucleus Interactions. *ACS Nano* **2012**, *6*, 3318.

(7) Han, S.; Liu, Y.; Nie, X.; Xu, Q.; Jiao, F.; Li, W.; Zhao, Y.; Wu, Y.; Chen, C. Efficient Delivery of Antitumor Drug to the Nuclei of Tumor Cells by Amphiphilic Biodegradable Poly (L-Aspartic Acid-Co-Lactic Acid)/Dppe Co-Polymer Nanoparticles. *Small* **2012**, *8*, 1596.

(8) Radhakrishnan, K.; Thomas, M. B.; Pulakkat, S.; Gnanadhas, D. P.; Chakravortty, D.; Raichur, A. M. Stimuli-Responsive Protamine-Based Biodegradable Nanocapsules for Enhanced Bioavailability and Intracellular Delivery of Anticancer Agents. *J. Nanopart. Res.* **2015**, *17*, 341.

(9) Vasir, J. K.; Labhasetwar, V. Quantification of the Force of Nanoparticle-Cell Membrane Interactions and Its Influence on Intracellular Trafficking of Nanoparticles. *Biomaterials* **2008**, *29*, 4244−4252.

(10) Huo, S.; Jin, S.; Ma, X.; Xue, X.; Yang, K.; Kumar, A.; Wang, P. C.; Zhang, J.; Hu, Z.; Liang, X.-J. Ultrasmall Gold Nanoparticles as Carriers for Nucleus-Based Gene Therapy Due to Size-Dependent Nuclear Entry. *ACS Nano* **2014**, *8*, 5852−5862.

(11) Pan, L.; He, Q.; Liu, J.; Chen, Y.; Ma, M.; Zhang, L.; Shi, J. Nuclear-Targeted Drug Delivery of Tat Peptide-Conjugated Monodisperse Mesoporous Silica Nanoparticles. *J. Am. Chem. Soc.* **2012**, *134*, 5722.

(12) Misra, R.; Sahoo, S. K. Intracellular Trafficking of Nuclear Localization Signal Conjugated Nanoparticles for Cancer Therapy. *Eur. J. Pharm. Sci.* **2010**, *39*, 152.

(13) Pradhan, L.; Srivastava, R.; Bahadur, D. Enhanced Anticancer Efficacy of Folate-Grafted Lipid Modified Dual Drug Loaded Nanoassemblies to Reduce Drug Resistance in Ovarian Cancer. *Biomedical Physics & Engineering Express* **2016**, *2*, 065005.

(14) Dobrovolskaia, M. A.; McNeil, S. E. Immunological Properties of Engineered Nanomaterials. *Nat. Nanotechnol.* **2007**, *2*, 469.

(15) Jang, H.; Ryoo, S.-R.; Kostarelos, K.; Han, S. W.; Min, D.-H. The Effective Nuclear Delivery of Doxorubicin from Dextran-Coated Gold Nanoparticles Larger Than Nuclear Pores. *Biomaterials* **2013**, *34*, 3503.

(16) Li, Y. L.; Zhu, L.; Liu, Z.; Cheng, R.; Meng, F.; Cui, J. H.; Ji, S. J.; Zhong, Z. Reversibly Stabilized Multifunctional Dextran Nanoparticles Efficiently Deliver Doxorubicin into the Nuclei of Cancer Cells. *Angew. Chem., Int. Ed.* **2009**, *48*, 9914.

(17) Wang, C.; Wu, C.; Zhou, X.; Han, T.; Xin, X.; Wu, J.; Zhang, J.; Guo, S. Enhancing Cell Nucleus Accumulation and DNA Cleavage Activity of Anti-Cancer Drug Via Graphene Quantum Dots. *Sci. Rep.* **2013**, *3*, 2852.

(18) Soroory, H.; Mashak, A.; Rahimi, A. Application of Pdms-Based Coating in Drug Delivery Systems Using Pvp as Channeling Agent. *Iran. Polym. J.* **2013**, *22*, 791.

(19) Park, J. H.; Park, K. D.; Bae, Y. H. Pdms-Based Polyurethanes with Mpeg Grafts: Synthesis, Characterization and Platelet Adhesion Study. *Biomaterials* **1999**, *20*, 943.

(20) Goda, T.; Ishihara, K. Soft Contact Lens Biomaterials from Bioinspired Phospholipid Polymers. *Expert Rev. Med. Devices* **2006**, *3*, 167.

(21) Zullo, M. A.; Plotti, F.; Bellati, F.; Muzii, L.; Angioli, R.; Panici, P. B. Transurethral Polydimethylsiloxane Implantation: A Valid Option for the Treatment of Stress Urinary Incontinence Due to Intrinsic Sphincter Deficiency without Urethral Hypermobility. *J. Urol.* **2005**, *173*, 898.

(22) Chu, M. K.; Gordijo, C. R.; Li, J.; Abbasi, A. Z.; Giacca, A.; Plettenburg, O.; Wu, X. Y. In Vivo Performance and Biocompatibility of a Subcutaneous Implant for Real-Time Glucose-Responsive Insulin Delivery. *Diabetes Technol. Ther.* **2015**, *17*, 255−267.

(23) Guy, R. H.; Hadgraft, J. Transdermal Drug Delivery-a Perspective. *J. Controlled Release* **1987**, *4*, 237.

(24) Jain, S. K.; Gupta, Y.; Jain, A.; Rai, K. Enhanced Transdermal Delivery of Acyclovir Sodium Via Elastic Liposomes. *Drug Delivery* **2008**, *15* (3), 141−147.

DOI: 10.1021/acsami.7b08806
ACS Appl. Mater. Interfaces 2017, 9, 34625−34633

(25) Cevc, G. Transdermal Drug Delivery of Insulin with Ultradeformable Carriers. *Clin. Pharmacokinet.* **2003**, *42* (5), 461−474.
(26) Car, A.; Baumann, P.; Duskey, J. T.; Chami, M.; Bruns, N.; Meier, W. Ph-Responsive Pdms-B-Pdmaema Micelles for Intracellular Anticancer Drug Delivery. *Biomacromolecules* **2014**, *15*, 3235−3245.
(27) Di, C.; Jiang, X.; Wang, R.; Yin, J. Multi-Responsive Polymer Nanoparticles from the Amphiphilic Poly (Dimethylsiloxane)(Pdms)-Containing Poly (Ether Amine)(Pdms-Gpea) and Its Potential Application for Smart Separation. *J. Mater. Chem.* **2011**, *21*, 4416−4423.
(28) Wang, Y.; Bansal, V.; Zelikin, A. N.; Caruso, F. Templated Synthesis of Single-Component Polymer Capsules and Their Application in Drug Delivery. *Nano Lett.* **2008**, *8*, 1741−1745.
(29) Björnmalm, M.; Cui, J.; Bertleff-Zieschang, N.; Song, D.; Faria, M.; Rahim, M. A.; Caruso, F. Nanoengineering Particles through Template Assembly. *Chem. Mater.* **2017**, *29*, 289.
(30) Buchel, G.; Unger, K. K.; Matsumoto, A.; Tsutsumi, K. A Novel Pathway for Synthesis of Submicrometer-Size Solid Core/Mesoporous Shell Silica Spheres. *Adv. Mater.* **1998**, *10*, 1036.
(31) Jothimuthu, P.; Carroll, A.; Bhagat, A. A. S.; Lin, G.; Mark, J. E.; Papautsky, I. Photodefinable Pdms Thin Films for Microfabrication Applications. *J. Micromech. Microeng.* **2009**, *19*, 045024.
(32) David-Beabes, G. L.; Overman, M. J.; Petrofski, J. A.; Campbell, P. A.; Demarzo, A. M.; Nelson, W. G. Doxorubicin-Resistant Variants of Human Prostate Cancer Cell Lines Du 145, Pc-3, Ppc-1, and Tsu-Pr1: Characterization of Biochemical Determinants of Antineoplastic Drug Sensitivity. *Int. J. Oncol.* **2000**, *17* (6), 1077−1086.
(33) Cypryk, M.; Apeloig, Y. Mechanism of the Acid-Catalyzed Si−O Bond Cleavage in Siloxanes and Siloxanols. A Theoretical Study. *Organometallics* **2002**, *21* (11), 2165−2175.
(34) Mosmann, T. Rapid Colorimetric Assay for Cellular Growth and Survival: Application to Proliferation and Cytotoxicity Assays. *J. Immunol. Methods* **1983**, *65*, 55.
(35) Barnes, C. A.; Elsaesser, A.; Arkusz, J.; Smok, A.; Palus, J.; Lesniak, A.; Salvati, A.; Hanrahan, J. P.; Jong, W. H. d.; Dziubałtowska, E.; et al. Reproducible Comet Assay of Amorphous Silica Nanoparticles Detects No Genotoxicity. *Nano Lett.* **2008**, *8*, 3069.
(36) Yang, K.; Xu, H.; Cheng, L.; Sun, C.; Wang, J.; Liu, Z. In Vitro and in Vivo near-Infrared Photothermal Therapy of Cancer Using Polypyrrole Organic Nanoparticles. *Adv. Mater.* **2012**, *24* (41), 5586−5592.
(37) Farokhzad, O. C.; Cheng, J.; Teply, B. A.; Sherifi, I.; Jon, S.; Kantoff, P. W.; Richie, J. P.; Langer, R. Targeted Nanoparticle-Aptamer Bioconjugates for Cancer Chemotherapy in Vivo. *Proc. Natl. Acad. Sci. U. S. A.* **2006**, *103* (16), 6315−6320.

DOI: 10.1021/acsami.7b08806
ACS Appl. Mater. Interfaces 2017, 9, 34625−34633